

Theory of Diamagnetism in the Pseudogap Phase: Implications from the Self energy of Angle Resolved Photoemission

Dan Wulin and K. Levin

*James Franck Institute and Department of Physics,
University of Chicago, Chicago, Illinois 60637, USA*

(Dated: November 10, 2018)

In this paper we apply the emerging- consensus understanding of the fermionic self energy deduced from angle resolved photoemission spectroscopy (ARPES) experiments to deduce the implications for orbital diamagnetism in the underdoped cuprates. Many theories using many different starting points have arrived at a broadened BCS-like form for the normal state self energy associated with a d -wave excitation gap, as is compatible with ARPES data. Establishing compatibility with the f-sum rules, we show how this self energy, along with the constraint that there is no Meissner effect in the normal phase are sufficient to deduce the orbital susceptibility. We conclude, moreover, that diamagnetism is large for a d -wave pseudogap. Our results should apply rather widely to many theories of the pseudogap, independent of the microscopic details.

PACS numbers:

INTRODUCTION

The origin of the pseudogap in high temperature superconductors is still very much under debate. While there are indications of an alternative order parameter [1, 2] it is widely accepted that the diamagnetism which is associated with the pseudogap is indicative of some form of precursor pairing. Nevertheless, even within the various schools which posit preformed pairs there is controversy about their nature and origin. What would be particularly useful, given this multitude of scenarios is to build an understanding of the pseudogap phase based on aspects of phenomenological (and microscopic) theories about which there is some degree of convergence.

In this paper we focus on the diamagnetism of the cuprates (in the linear response regime) and show how it is connected to an emerging- consensus understanding [3–6] of angle resolved photoemission experiments. These experiments have demonstrated that a simple broadened BCS form for the self energy in the presence of a pseudogap $\Delta_{pg,\mathbf{k}}$

$$\Sigma_{pg,K} = -i\gamma + \frac{\Delta_{pg,\mathbf{k}}^2}{i\omega_n + \xi_{\mathbf{k}} + i\gamma} \quad (1)$$

works rather well. Indeed, this form of the self energy is widely subscribed to [3–6] in diverse theories of the pseudogap. Here we exploit this equation (and the related fermiology constraining the bandstructure $\xi_{\mathbf{k}}$) in conjunction with the important constraint that there is no Meissner effect in the pseudogap phase, to arrive at a form for the orbital susceptibility. This relation between transport and self energy is well known from the Ward identities. In a closely related fashion we justify our transport expressions for the diamagnetic response by showing that the related current-current correlation function analytically satisfies the transverse and longitu-

dinal f-sum rules. In this sense this understanding of diamagnetism should have a generality which goes beyond a particular microscopic or phenomenological approach.

Recent experiments measuring the orbital susceptibility in a variety of cuprate superconductors report anomalously large diamagnetism [7, 8]). This diamagnetism onset is well correlated with the onset of an enhanced Nernst signal above T_c in the same materials [9]. It is not likely that low dimensional, critical fluctuations are responsible, because the diamagnetism persists beyond the expected critical regime. Moreover, there are reports of strong non-linear effects, although they will not be the topic of this paper.

This pseudogap phase has been very systematically studied in angle resolved photoemission spectroscopy (ARPES) experiments which lead to the phenomenological expression in Eq. (1) as well as the underlying fermiology. An important feature in the precursor superconductivity approaches is the Fermi “arcs”, (as distinguished from Fermi “pockets”). These are understood to arise from the phenomenological broadening factor γ in Eq. (1) which leads to a smearing out of the d -wave nodes. Also relevant are the collapse of the arcs below T_c and the related “two gap” phenomena which appear in the superconducting phase. Importantly, they follow naturally [10, 11] from Eq. (1) if one adds to Σ_{pg} a co-existing conventional condensate contribution Σ_{sc} , (of the same form but with the order parameter contribution, Δ_{sc}^2 appearing and the associated $\gamma = 0$). Theoretical approaches to diamagnetism have not incorporated this ARPES constraint, largely because they are based on thermodynamic rather than transport schemes. Moreover, for the most part the emphasis has been on the contribution of bosonic pairs either in fluctuation [12–14] or real space pairing schemes. [15]. Nevertheless, physically, one might expect the total diamagnetic response to

reflect fermions as well as these pair correlations. Indeed, this has to be crucial when the fermionic self energy is incorporated and sum rules are addressed. Alternative theories based on vortex liquids [16] or d-density wave states [17] have addressed complementary physics.

Overview of Theory and Results

It is useful to begin with an overview of the connection between ARPES and diamagnetism. The reasoning is relatively simple and is best communicated by presenting the theory first in summary form.

For the sake of notational simplicity, the equations we present here are for the negligibly small γ limit, although the general line of reasoning can readily accomodate any size γ , as discussed in the Appendix. The transport-based expression for the diamagnetic response is

$$\chi^{\text{dia}} = - \lim_{q_y \rightarrow 0} \text{Re} \left[\frac{P_{xx}(\mathbf{q}, \omega = 0) + (n/m)_{xx}}{\mathbf{q}^2} \right]_{q_x=q_z=0} \quad (2)$$

Here χ^{dia} is written in terms of the current-current correlation function $\overleftrightarrow{P}(\mathbf{q}, \omega)$ and the diamagnetic current tensor \overleftarrow{n}/m . The absence of a Meissner effect is equivalent to the vanishing of the electromagnetic response kernel above T_c at zero momentum and frequency, i.e. the response kernel must satisfy

$$\overleftrightarrow{P}(0, 0) + \frac{\overleftarrow{n}}{m} = 0, T \geq T_c \quad (3)$$

When Eq.3 is satisfied, the first nonzero term in the numerator of Eq.2 comes in at $\mathcal{O}(\mathbf{q}^2)$, rendering χ^{dia} well-behaved. The analogue statement below T_c is that the right hand side of Eq.3 equals \overleftarrow{n}_s/m , the superfluid density tensor.

It is helpful to recast the expression for \overleftarrow{n}/m in a way that closely mirrors the structure of a response function:

$\frac{\overleftarrow{n}}{m} = 2 \sum_K \frac{\partial^2 \xi_{\mathbf{k}}}{\partial \mathbf{k} \partial \mathbf{k}} G_K$ can be rewritten after some straightforward algebra as

$$\overleftrightarrow{P}(0, 0) = 2 \sum_K \frac{\partial \xi_{\mathbf{k}}}{\partial \mathbf{k}} \frac{\partial \xi_{\mathbf{k}}}{\partial \mathbf{k}} G_K^2 \left(1 - \Delta_{pg, \mathbf{k}}^2 G_{0, -K}^2 \right) \quad (4)$$

Now let us consider the relation to Landau diamagnetism. Ignoring lattice effects for the moment, the standard expression for the orbital susceptibility is of the form ([18, 19])

$$\chi^{\text{dia}} \propto \frac{-n}{m} \frac{e^2}{c^2} \langle \mathbf{r}^2 \rangle \quad (5)$$

where n and m represent the density and mass of the charge carriers in Landau orbits. The source of large

conventional fluctuation diamagnetism [12] is the characteristic size $\langle \mathbf{r}^2 \rangle$ which is presumed equal to the correlation length and which diverges as the transition is approached. Consequently, even in the absence of fluctuations, one might expect that s -wave pairs would have significantly less diamagnetism than the more extended d -wave pairs of the cuprates, as we demonstrate here.

We will show that the orbital susceptibility deriving from Eq. (1) arises from both fermionic and bosonic contributions. Diamagnetism comes predominantly from the latter and one can understand this physically as associated with the general enhancement of bosonic contributions to transport in the vicinity of Bose condensation. A strongly peaked Bose distribution function (in momentum space) readily accomodates a redistribution of particles leading to large transport responses even in the presence of weak perturbing fields. Indeed, this is the origin of superconducting fluctuation contributions, in general. This is in contrast to fermionic transport, which is restricted by the Pauli principle.

We note that [20] even in a zero gap normal state, bandstructure effects can yield a paramagnetic orbital susceptibility, particularly near Van Hove singularities. Thus one might expect the net diamagnetic contribution will be largest away from the Van Hove points. An additional effect of the fermionic contribution derives from the fact that an excitation gap will reduce the number of available fermions n . Because of nodal fermions, d -wave pairing in the pseudogap phase is expected to yield more diamagnetism. In this paper we will show how all of these effects combine to yield a rather large diamagnetic response strongly associated with a d -wave pseudogap.

We present in this introduction an important inference which will be discussed in more detail later and which allows us to arrive at an extension of Eq.4 to finite momentum and frequency in the form

$$\overleftrightarrow{P}(\mathbf{q}, i\Omega_m) = 2 \sum_K \frac{\partial \xi_{\mathbf{k}+\mathbf{q}/2}}{\partial \mathbf{k}} \frac{\partial \xi_{\mathbf{k}+\mathbf{q}/2}}{\partial \mathbf{k}} \left[G_K G_{K+Q} - \Delta_{pg, \mathbf{k}} \Delta_{pg, \mathbf{k}+\mathbf{q}} G_{0, -K-Q} G_{0, -K} G_{K+Q} G_K \right] \quad (6)$$

One could anticipate such an answer using the standard normal state expression for the current-current correlation function (c.f. [21]) or alternatively the counterpart for the standard BCS current-current correlation function (where one has to be careful to enforce a Meissner effect, rather than its absence in the pseudogap phase). But the strongest support for Eq. (6) is the demonstration that it analytically satisfies the f-sum rules. These are discussed in more detail in Appendix A. Importantly Eq. (6) provides the input one needs to arrive at transport properties (including the complex conductivity) that arise from Ward identity compatibility with the ARPES-derived self energy.

It is useful to end this introduction with a summary figure addressing the implications of the pseudogap as

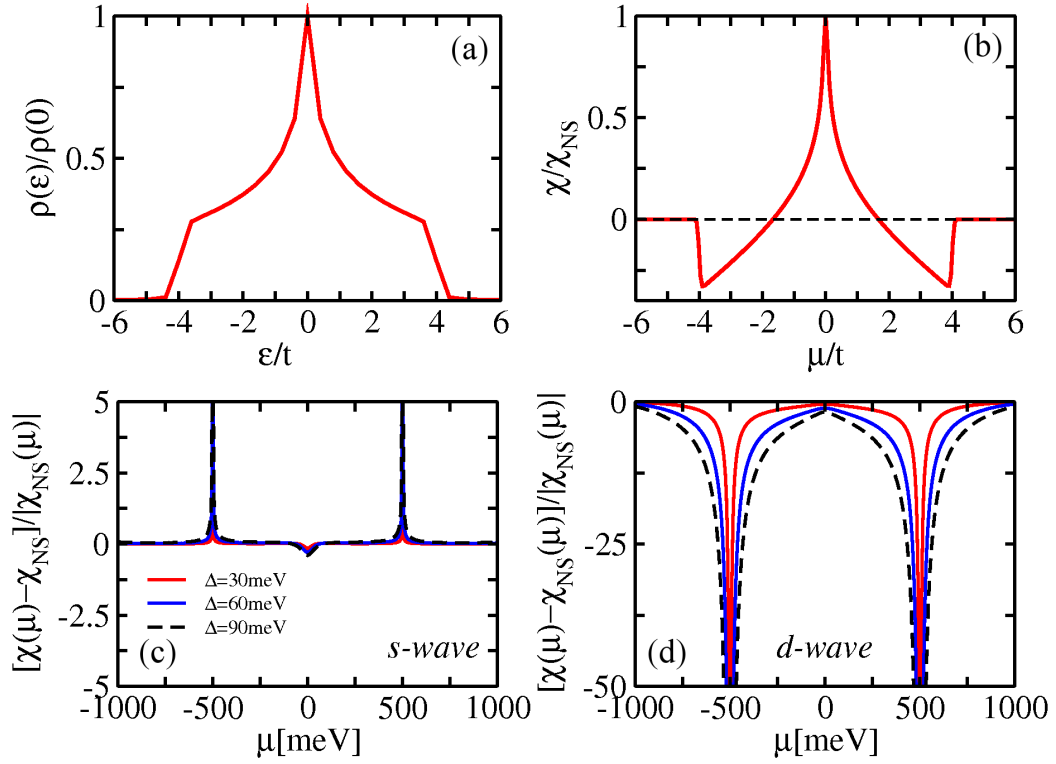


Figure 1: Summary Figure showing the effect of the pseudogap for *s* and *d*-wave lattices via plots as functions of band filling or chemical potential, μ . (a) corresponds to the assumed density of states, (b) to the normal state susceptibility while (c) and (d) illustrate the difference between the pseudogap and normal state χ^{dia} normalized by the absolute value of χ^{dia} in the normal state at the same μ . In (c) the pseudogap is taken to have an *s*-wave form factor. (d) The analogous plot but for a *d*-wave order parameter.

it appears in Eq. (1) on the orbital susceptibility. The four panels in this figure correspond to (a) the assumed density of states as a function of energy and (b) the counterpart normal state orbital susceptibility as a function of band filling. Note that the simple Landau diamagnetism of jellium can give rise to paramagnetism in a tight binding band, particularly near Van Hove singularities. In (c) we indicate the *change* in the orbital susceptibility associated with the pseudogap as a function of band filling for *s*-wave pairing. The counterpart figure for the *d*-wave case is shown in (d). A comparison shows that the *d*-wave pseudogap is associated with substantially enhanced diamagnetism. This figure will be discussed in more detail in the context of our numerical results.

THEORY OF DIAMAGNETIC SUSCEPTIBILITY

We begin by rewriting the expression for \overleftrightarrow{n}/m :

$$= -2 \sum_K \frac{\partial \xi_{\mathbf{k}}}{\partial \mathbf{k}} \frac{\partial G_K}{\partial \mathbf{k}} \quad (7)$$

following an integration by parts. Next we rewrite the derivative of the Green's function using the identity

$\partial G_K / \partial \mathbf{k} = -G_K^2 \partial G_K^{-1} / \partial \mathbf{k}$, where the derivative of the inverse Green's function is straightforward to evaluate in terms of the ARPES-derived $\Sigma_{pg,K}$,

$$\frac{\partial G_{\mathbf{k}}^{-1}}{\partial \mathbf{k}} = \frac{\partial G_{0,K}^{-1}}{\partial \mathbf{k}} - \frac{\partial \Sigma_{pg,K}}{\partial \mathbf{k}} = -\frac{\partial \xi_{\mathbf{k}}}{\partial \mathbf{k}} - \frac{\partial \Sigma_{pg,K}}{\partial \mathbf{k}} \quad (8)$$

From Eq.3, the current-current correlation function at $\mathbf{q}, i\Omega = 0$ necessarily yields Eq.4.

The structure of Eq.4 is intriguing: the first term in parenthesis is the usual electromagnetic response of fermionic quasiparticles, while the second term arises from the presence of pseudogap correlations and has the appearance of being a correction to the bare electromagnetic vertex.

We then posit Eq.6 as the natural extension to arbitrary four-vector Q , and this is supported by the transverse and longitudinal f-sum rules. For the latter we have to prove the longitudinal and transverse f-sum rules. Previously [22, 23] we have focused on the second of these, which will be summarized here in the Appendix. We now address the longitudinal sum rule

$$\int_{-\infty}^{+\infty} \frac{d\omega}{\pi} \left(-\frac{\text{Im} \chi_{JJ}^L(\omega, \mathbf{q})}{\omega} \right) = \frac{n}{m}, \quad (9)$$

We define $f^\pm \equiv f(E_{\mathbf{k}})$ as the fermi function, $E^\pm \equiv E_{\mathbf{k} \pm \mathbf{b}f_{q/2}}$, $\xi^\pm \equiv \xi_{\mathbf{k} \pm \mathbf{q}/2}$, and $\Delta_{pg}^\pm \equiv \Delta_{pg, \mathbf{k} \pm \mathbf{q}/2}$. The normal state fermions have dispersion $E_{\mathbf{k}} \equiv \sqrt{\xi_{\mathbf{k}}^2 + \Delta_{pg}^2(T)}$. The longitudinal component of $\vec{\chi}_{JJ}$ is defined as $\chi_{JJ}^L \equiv \hat{\mathbf{q}} \cdot \vec{\chi}_{JJ} \cdot \hat{\mathbf{q}} = \mathbf{q} \cdot \vec{\chi}_{JJ} \cdot \mathbf{q}/q^2$. We need several simple relations

$$\begin{aligned} \text{Im} \frac{1}{\omega \pm (E_{\mathbf{p}}^+ \pm E_{\mathbf{p}}^-) + i\delta} &= -\pi \delta(\omega \pm (E_{\mathbf{p}}^+ \pm E_{\mathbf{p}}^-)), \\ \frac{\mathbf{p} \cdot \mathbf{q}}{m} &= \xi_{\mathbf{p}}^+ - \xi_{\mathbf{p}}^- \end{aligned} \quad (10)$$

along with

$$\begin{aligned} &(\xi_{\mathbf{p}}^+ - \xi_{\mathbf{p}}^-)(E_{\mathbf{p}}^+ E_{\mathbf{p}}^- - \xi_{\mathbf{p}}^+ \xi_{\mathbf{p}}^- + \Delta_{pg}^2) \\ &= (\xi_{\mathbf{p}}^+ E_{\mathbf{p}}^- - \xi_{\mathbf{p}}^- E_{\mathbf{p}}^+)(E_{\mathbf{p}}^+ + E_{\mathbf{p}}^-), \quad \text{and} \quad , \end{aligned} \quad (11)$$

$$\begin{aligned} &(\xi_{\mathbf{p}}^+ - \xi_{\mathbf{p}}^-)(E_{\mathbf{p}}^+ E_{\mathbf{p}}^- + \xi_{\mathbf{p}}^+ \xi_{\mathbf{p}}^- - \Delta_{pg}^2) \\ &= (\xi_{\mathbf{p}}^+ E_{\mathbf{p}}^- + \xi_{\mathbf{p}}^- E_{\mathbf{p}}^+)(E_{\mathbf{p}}^+ - E_{\mathbf{p}}^-). \end{aligned} \quad (12)$$

We have

$$\begin{aligned} &\int_{-\infty}^{+\infty} \frac{d\omega}{\pi} \left(-\frac{\text{Im} \chi_{JJ}^L(\omega, \mathbf{q})}{\omega} \right) \\ &= \sum_{\mathbf{p}} \frac{\mathbf{p} \cdot \mathbf{q} (\xi_{\mathbf{p}}^+ - \xi_{\mathbf{p}}^-)}{mq^2} \left\{ \frac{E_{\mathbf{p}}^+ E_{\mathbf{p}}^- - \xi_{\mathbf{p}}^+ \xi_{\mathbf{p}}^- + \Delta_{pg}^2}{E_{\mathbf{p}}^+ E_{\mathbf{p}}^-} \frac{1}{E_{\mathbf{p}}^+ + E_{\mathbf{p}}^-} [1 - f(E_{\mathbf{p}}^+) - f(E_{\mathbf{p}}^-)] \right. \\ &\quad \left. - \frac{E_{\mathbf{p}}^+ E_{\mathbf{p}}^- + \xi_{\mathbf{p}}^+ \xi_{\mathbf{p}}^- - \Delta_{pg}^2}{E_{\mathbf{p}}^+ E_{\mathbf{p}}^-} \frac{1}{E_{\mathbf{p}}^+ - E_{\mathbf{p}}^-} [f(E_{\mathbf{p}}^+) - f(E_{\mathbf{p}}^-)] \right\}, \end{aligned} \quad (13)$$

This yields

$$\begin{aligned} &\int_{-\infty}^{+\infty} \frac{d\omega}{\pi} \left(-\frac{\text{Im} \chi_{JJ}^L(\omega, \mathbf{q})}{\omega} \right) \\ &= \sum_{\mathbf{p}} \frac{\mathbf{p} \cdot \mathbf{q}}{mq^2} \left[\frac{\xi_{\mathbf{p}}^+}{E_{\mathbf{p}}^+} (1 - 2f(E_{\mathbf{p}}^+)) - \frac{\xi_{\mathbf{p}}^-}{E_{\mathbf{p}}^-} (1 - 2f(E_{\mathbf{p}}^-)) \right] \\ &= \sum_{\mathbf{p}} \frac{\mathbf{p} \cdot \mathbf{q}}{mq^2} \left[1 - \frac{\xi_{\mathbf{p}}^-}{E_{\mathbf{p}}^-} (1 - 2f(E_{\mathbf{p}}^-)) \right] - \sum_{\mathbf{p}} \frac{\mathbf{p} \cdot \mathbf{q}}{mq^2} \left[1 - \frac{\xi_{\mathbf{p}}^+}{E_{\mathbf{p}}^+} (1 - 2f(E_{\mathbf{p}}^+)) \right]. \end{aligned} \quad (14)$$

Changing variables $\mathbf{p} \rightarrow \mathbf{p} + \frac{\mathbf{q}}{2}$ for the first and $\mathbf{p} \rightarrow \mathbf{p} - \frac{\mathbf{q}}{2}$ for the second term, yields the desired result

$$\begin{aligned} &\int_{-\infty}^{+\infty} \frac{d\omega}{\pi} \left(-\frac{\text{Im} \chi_{JJ}^L(\omega, \mathbf{q})}{\omega} \right) \\ &= \sum_{\mathbf{p}} \frac{\mathbf{q} \cdot \mathbf{q}}{mq^2} \left[1 - \frac{\xi_{\mathbf{p}}}{E_{\mathbf{p}}} (1 - 2f(E_{\mathbf{p}})) \right] \\ &= \frac{1}{m} \sum_{\mathbf{p}} \left[1 - \frac{\xi_{\mathbf{p}}}{E_{\mathbf{p}}} (1 - 2f(E_{\mathbf{p}})) \right] \\ &= \frac{n}{m}. \end{aligned} \quad (15)$$

Explicit Calculation of Diamagnetic Susceptibility

The electromagnetic response kernel has been constructed so that there is no Meissner effect above T_c , only the q_y^2 coefficient in the series expansion of Eq.6 is needed to calculate χ^{dia} . The calculation is lengthy but straightforward, with the result that χ^{dia} can be written as the sum of two terms, $\chi^{\text{dia}} = \chi_0^{\text{dia}} + \delta\chi^{\text{dia}}$ where

$$\begin{aligned} \chi_0^{\text{dia}} &= -\sum_{\mathbf{k}} \left(\frac{\partial \xi_{\mathbf{k}}}{\partial k_x} \right)^2 \frac{1}{12E_{\mathbf{k}}^7} \left(3\Delta_{pg, \mathbf{k}}^2 \left(3m_{\mathbf{k}}^{-1} \xi_{\mathbf{k}} E_{\mathbf{k}}^2 + v_{\mathbf{k}}^2 [\Delta_{pg, \mathbf{k}}^2 - 4\xi_{\mathbf{k}}^2] \right) (1 - 2f(E_{\mathbf{k}})) \right. \\ &\quad + 6\Delta_{pg, \mathbf{k}}^2 E_{\mathbf{k}} \left(3m_{\mathbf{k}}^{-1} \xi_{\mathbf{k}}^3 + 3m_{\mathbf{k}}^{-1} \xi_{\mathbf{k}} \Delta_{pg, \mathbf{k}}^2 - 4\xi_{\mathbf{k}}^2 v_{\mathbf{k}}^2 + \Delta_{pg, \mathbf{k}}^2 v_{\mathbf{k}}^2 \right) f'(E_{\mathbf{k}}) \\ &\quad \left. + 6\xi_{\mathbf{k}}^2 E_{\mathbf{k}}^2 \left(m_{\mathbf{k}}^{-1} \xi_{\mathbf{k}} E_{\mathbf{k}}^2 + 2\Delta_{pg, \mathbf{k}}^2 v_{\mathbf{k}}^2 \right) f''(E_{\mathbf{k}}) + 2\xi_{\mathbf{k}}^4 E_{\mathbf{k}}^3 v_{\mathbf{k}}^2 f^{(3)}(E_{\mathbf{k}}) \right) \quad \text{and} \end{aligned} \quad (16)$$

$$\begin{aligned}
\delta\chi^{\text{dia}} = & -\sum_{\mathbf{k}} \left(\frac{\partial \xi_{\mathbf{k}}}{\partial k_x} \right)^2 \frac{1}{12E_{\mathbf{k}}^7} \left(\left(\frac{\partial \phi_{\mathbf{k}}}{\partial k_y} \right)^2 (15\xi_{\mathbf{k}}^2 \Delta_{pg,\mathbf{k}}^2 [1 - 2f(E_{\mathbf{k}})] + 30\xi_{\mathbf{k}}^2 \Delta_{pg,\mathbf{k}}^2 E_{\mathbf{k}} f'(E_{\mathbf{k}})) \right. \\
& + 6E_{\mathbf{k}}^2 (\xi_{\mathbf{k}}^4 + \Delta_{\mathbf{k}}^4) f''(E_{\mathbf{k}}) + 2E_{\mathbf{k}}^3 \xi_{\mathbf{k}}^2 \Delta_{pg,\mathbf{k}}^2 f^{(3)}(E_{\mathbf{k}})) \\
& - \frac{1}{6E_{\mathbf{k}}^7} \xi_{\mathbf{k}} \Delta_{pg,\mathbf{k}} v_{\mathbf{k}} \frac{\partial \varphi_{\mathbf{k}}}{\partial k_y} ([6\xi_{\mathbf{k}}^2 - 9\Delta_{pg,\mathbf{k}}^2] (1 - 2f(E_{\mathbf{k}})) + 6(2\xi_{\mathbf{k}}^2 - 3\Delta_{pg,\mathbf{k}}^2) E_{\mathbf{k}} f'(E_{\mathbf{k}})) \\
& - 6E_{\mathbf{k}}^2 (\xi_{\mathbf{k}}^2 - \Delta_{pg,\mathbf{k}}^2) f''(E_{\mathbf{k}}) + 2E_{\mathbf{k}}^3 \xi_{\mathbf{k}}^2 f^{(3)}(E_{\mathbf{k}})) \\
& - \frac{\Delta_{pg,\mathbf{k}}}{4E_{\mathbf{k}}^5} \frac{\partial^2 \phi_{\mathbf{k}}}{\partial k_y^2} ((\Delta_{pg,\mathbf{k}}^2 - 2\xi_{\mathbf{k}}^2) (1 - 2f(E_{\mathbf{k}})) + 2(\Delta_{pg,\mathbf{k}}^2 - 2\xi_{\mathbf{k}}^2) E_{\mathbf{k}} f'(E_{\mathbf{k}})) \\
& \left. + 2\xi_{\mathbf{k}}^2 E_{\mathbf{k}}^2 f''(E_{\mathbf{k}}) \right) \quad (17)
\end{aligned}$$

Here we have separated terms so that the first is the contribution independent of derivatives of the gap form factor, while the second term introduces these derivative contributions, which are notably absent in the s -wave case. In the above equations we have $v_{\mathbf{k}}^2 = \frac{1}{2}(1 - \frac{\xi_{\mathbf{k}}}{E_{\mathbf{k}}})$ and $m_{\mathbf{k}}^{-1} \equiv \partial^2 \xi_{\mathbf{k}} / \partial k_x^2$.

The expressions Eq.16-17 are quite complicated, but general inferences can still be made on the expected behavior of the orbital susceptibility. We find that to a good approximation Eq.16 can be written as

$$\begin{aligned}
\chi_0^{\text{dia}} \approx & -\sum_{\mathbf{k}} \left(\frac{\partial \xi_{\mathbf{k}}}{\partial k_x} \right)^2 \frac{1}{4\Delta_{pg,\mathbf{k}}^4} \left(|\Delta_{pg,\mathbf{k}}| v_{\mathbf{k}}^2 (1 - 2f(|\Delta_{pg,\mathbf{k}}|)) \right. \\
& \left. + 2\Delta_{pg,\mathbf{k}}^2 v_{\mathbf{k}}^2 f'(|\Delta_{pg,\mathbf{k}}|) \right) \quad (18)
\end{aligned}$$

and Eq.17 is well approximated as

$$\begin{aligned}
(\delta\chi^{\text{dia}})_0 \approx & -\sum_{\mathbf{k}} \left(\frac{\partial \xi_{\mathbf{k}}}{\partial k_x} \right)^2 \left(\frac{1}{2} \left(\frac{\partial \phi_{\mathbf{k}}}{\partial k_y} \right)^2 \frac{f''(|\Delta_{pg,\mathbf{k}}|)}{2|\Delta_{pg,\mathbf{k}}|} \right. \\
& + \frac{1}{4\Delta_{pg,\mathbf{k}}^3} \frac{\partial^2 \varphi_{\mathbf{k}}}{\partial k_y^2} (|\Delta_{pg,\mathbf{k}}| (1 - 2f(|\Delta_{pg,\mathbf{k}}|)) \\
& \left. + 2\Delta_{pg,\mathbf{k}}^2 f'(|\Delta_{pg,\mathbf{k}}|)) \right) \quad (19)
\end{aligned}$$

It is seen from a numerical analysis that the largest contributing term to this last equation is the $(\partial \phi_{\mathbf{k}} / \partial k_y)^2$ piece.

NUMERICAL RESULTS

The sum of Equations (18) and (19) provides a reasonable approximation to the total orbital susceptibility Eq. (16)-(17). Moreover all that is needed is a the temperature dependent pseudogap parameter (and the chemical potential). It is our intention to first present results

that are independent of microscopic details so the plots are representative of general theories in which we treat Δ_{pg} and μ as variables. We will simultaneously consider s and d -wave pairing in both jellium and tight binding lattice models. For the latter we consider the simplest dispersion

$$\xi_{\mathbf{k}} = -2t(\cos(k_x) + \cos(k_y)) - 4t' \cos(k_x) \cos(k_y) - \mu(20)$$

along with more realistic fits to the cuprate bandstructure via ARPES data.

Jellium models with s and d -wave pairing

We begin by studying a jellium dispersion and an s -wave gap which avoids the complications of lattice effects and gap nodes. In Fig.2(a) we plot the orbital susceptibility from Eq.2. Curves are shown for $\Delta_{pg} = 0, 0.6$, and $1.2E_F$ and normalized by χ_{NS} , defined as the absolute value of the normal state orbital susceptibility when $\mu = 0$. The system exhibits diamagnetism even in the normal state, reflecting the well-known Landau orbital susceptibility corresponding to minus one third of the Pauli susceptibility. The degree of diamagnetism is increased modestly as the gap size increases; this numerically confirms the intuition that the bosonic term in Eq.6 results in an enhancement of χ^{dia} .

For the case of a d -wave gap with a jellium dispersion we use $\Delta_{pg,\mathbf{k}} = \Delta_{pg} \cos 2\phi$ where ϕ is the azimuthal angle. The resulting plot is shown in Fig.2(b). The curves are again displayed for $\Delta_{pg} = 0, 0.6$, and $1.2E_F$ and normalized by χ_{NS} . In contrast to the s -wave case, where χ grows as large as $\chi^{\text{dia}} \propto 3.5\chi_{NS}$, $\chi^{\text{dia}} \propto 17.5\chi_{NS}$ in the d -wave case, is roughly an order of magnitude larger than the normal state orbital susceptibility.

We understand this contrast between the s and d -wave order parameters as physically resulting from the

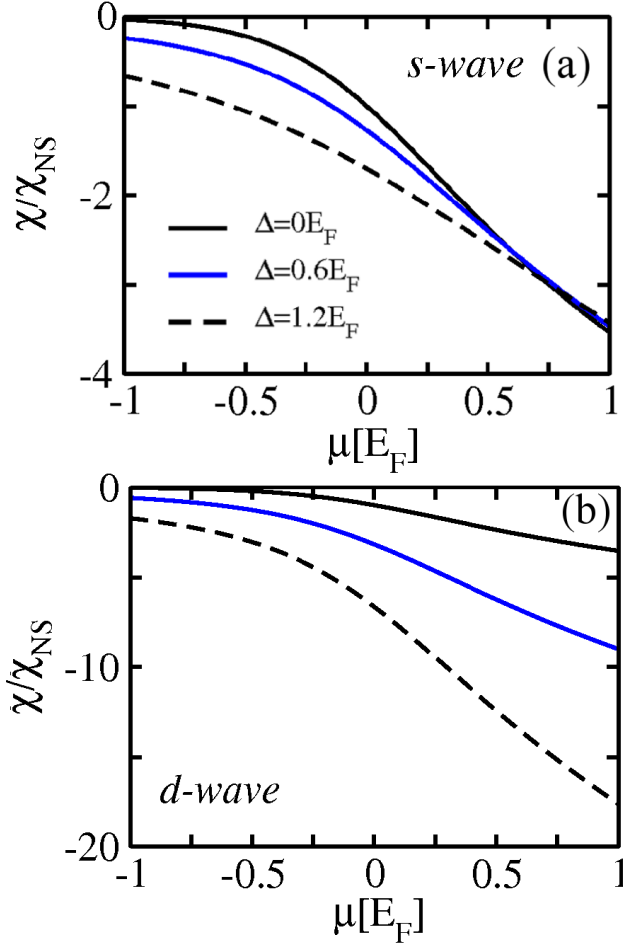


Figure 2: The orbital susceptibility for a jellium dispersion with an s-wave (upper) and d-wave gap (lower). We consider $\Delta_{pg} = 0, 0.6$, and $1.2E_F$. The curves are normalized by χ_{NS} , which is defined as the magnitude of the normal state value of χ^{dia} at $\mu = 0$. There is a finite orbital susceptibility even in the normal state. The diamagnetism is enhanced for all μ as size of the gap is increased. The d-wave gap symmetry results in a larger χ^{dia} than in the s-wave case.

increased pair size of the latter [24, 25], as reflected in the generic expression for orbital diamagnetism (Eq.5). The increased pair size reflects the nodal structure of the gaps; the correlation length of the pairs (which is *not* necessarily the same order of magnitude as the pair size) has a similar increase due to the nodes. It can be argued that the correlation length $\xi \propto \Delta_{FS}^{-1}$ where Δ_{FS} is the average of the gap along the Fermi surface. The quantity Δ_{FS} will always be less relative to an s-wave order parameter as long as the gap maximum is set to the same value as the s-wave gap that it is being compared against.

Fig.3 shows the change in the orbital susceptibility associated with a pseudogap for the case of jellium. Here we plot $\delta\chi_{NS} = \chi(\mu) - \chi_{NS}(\mu)$ normalized by $|\chi_{NS}(\mu)|$ for the gap values $\Delta_{pg} = 0.6$, and $1.2E_F$, where the normal

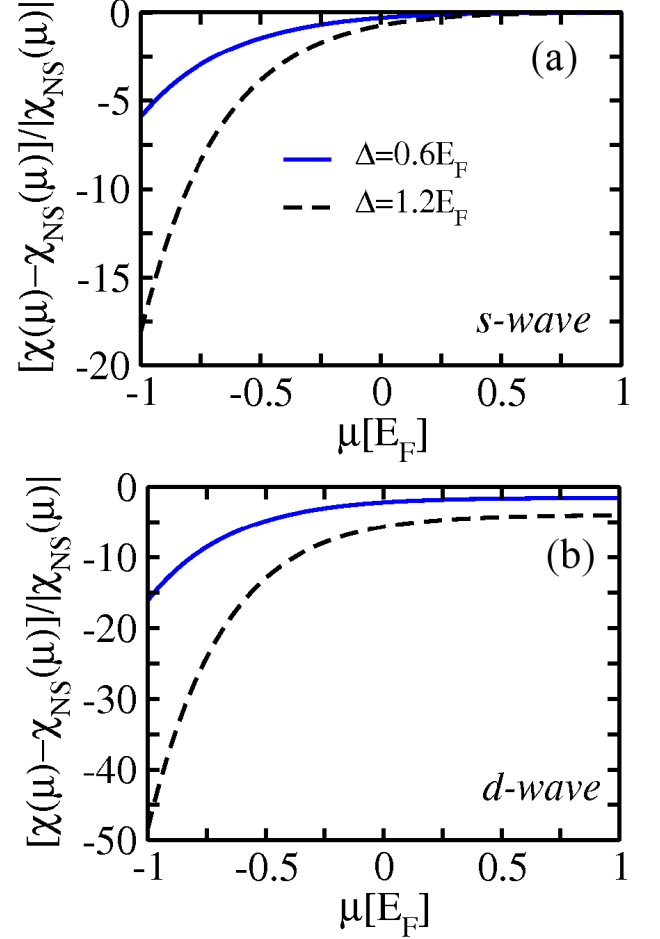


Figure 3: Change in the orbital susceptibility with varying pseudogap for a jellium dispersion. Plotted is the relative difference between the pseudogap and normal state χ^{dia} as a function of chemical potential μ for $\Delta = 0.6$, and $1.2E_F$. Upper panel is for an s-wave and lower panel for a d-wave gap. The presence of a pseudogap results in an increase of χ^{dia} for all values of μ . The trends as a function of μ and Δ are the same but the overall magnitude of the enhancement is more significant for the d-wave case.

state susceptibility is at $\mu = 0$. We consider $\Delta_{pg} = 0.6$ and $1.2E_F$ for the blue and black-dashed curves respectively. Fig.3(a) shows $\delta\chi_{NS}$ for an s-wave order parameter and Fig.3(b) plots the counterpart figure, $\delta\chi_{NS}$, for the d-wave case. For both the s and d wave cases when the filling is decreased (so the the normal state Landau orbital susceptibility is smallest) then the relative effect of the pseudogap appears more prominently. As anticipated, the overall diamagnetic contribution due to the d-wave order parameter is significantly larger than the contribution occurring for an s-wave pseudogap.

In summary, for a jellium dispersion, we have seen that (i) the presence of a pseudogap leads to an enhancement of the normal state diamagnetism for most values of the chemical potential μ . Critically, (ii) a d-wave order

Tight-binding lattice

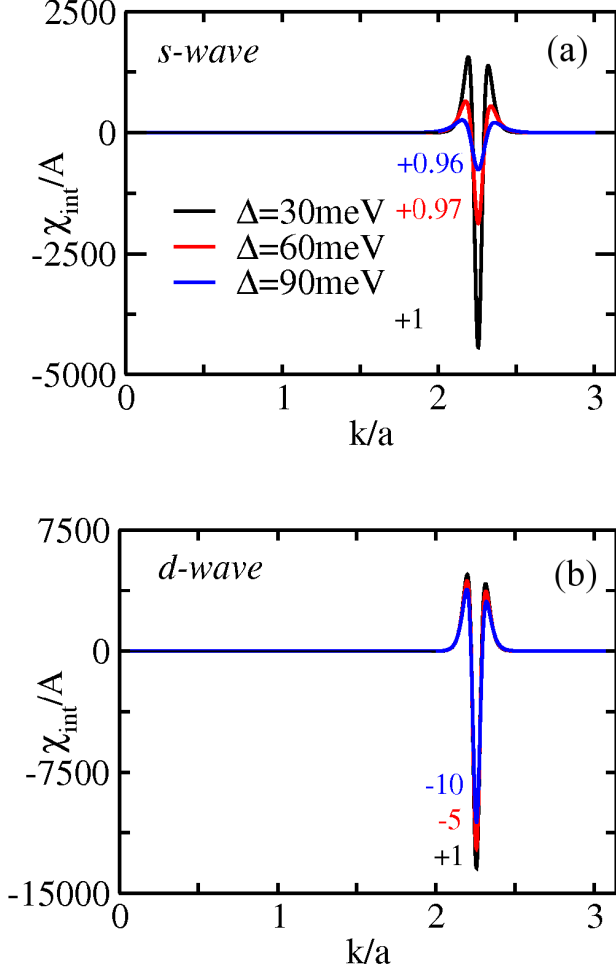


Figure 4: The orbital susceptibility integrand for a tight-binding dispersion at an angle $7\pi/36$ in the k_x - k_y plane. (top) The integrand for an s -wave order parameter of value $\Delta_{pg} = 30, 60$, and 90 meV. The curves are normalized by A , defined such that the area under the $\Delta_{pg} = 30$ meV curve is unity. The curve for all values of Δ_{pg} results in a paramagnetic contribution. The total area normalized by A of each curve is written alongside of it; the area takes the values 1, 0.97, and 0.96 for $\Delta_{pg} = 30, 60, 90$ meV respectively. (bottom) The same plots for a d -wave order parameter. The curve for $\Delta_{pg} = 60$ and 90 meV results in an overall diamagnetic contribution. The total area normalized by A of each curve is written alongside of it; the area takes the values 1, -5 , and -10 for $\Delta_{pg} = 30, 60, 90$ meV respectively.

parameter results in a significantly larger diamagnetism than in the case of an s -wave order parameter.

It is useful to understand the integrand before addressing the entire expression for the orbital susceptibility in a tight binding lattice. Figure 4 plots the integrand associated with Eq.16-17, as a function of radial distance in the k_x - k_y plane (normalized by the lattice spacing a). We consider three different values of the gap ($\Delta_{pg} = 30, 60$, and 90 meV). Each of the curves is normalized by a number A selected so that the curve corresponding to the smallest gap $\Delta_{pg} = 30$ meV has area unity; the area of the curves is noted beside each. All curves correspond to a cut at 35 degrees above the k_x axis. Fig.4(a) shows the integrand corresponding to an s -wave gap and Fig.4(b) corresponds to the d -wave case.

For the former these cuts result in paramagnetic contributions to χ^{dia} for all values of Δ_{pg} and the extent of the contribution is largely unchanged as Δ_{pg} increases: despite a tripling of the gap size, the displayed areas change by no more than 4% and lead to a paramagnetic contribution.

The corresponding curves for a d -wave order parameter are displayed in Fig. 4(b). Although the form of the curve does not change qualitatively as the gap size is changed, the initial area of the curve is sufficiently small such that minor changes to the cuts result in significant changes to the nature of the overall contribution to χ^{dia} : as the gap increases from 30 to 90 meV, the overall contribution changes from being paramagnetic to being 10 times as large and diamagnetic. This trend is driven by the d -wave gap symmetry.

We now return to Fig.1 which plots the density of states versus energy (a) and the orbital susceptibilities in the gapless normal state (b) and in the presence (c) of an s - or (d) a d wave pairing. The last three panels are plots as a function of band filling or chemical potential and the units are in terms of t , the nearest neighbor coupling which is taken to be 300 meV. Panel (b) shows that when $|\mu|$ is large, the density of holes or electrons is sufficiently small such that the system behaves similarly to the jellium case and χ^{dia} leads to the usual Landau orbital susceptibility result. There is a competition [20], however, between the E_F and t energy scales, so that once $|E_F|/t \leq 1.8$ the system becomes entirely paramagnetic. The term that contributes to this paramagnetism is weighted by the density of states evaluated at the Fermi surface and so it is dramatically enhanced by the Van-Hove point at $E_F = 0$. It is clear from the figure that the pseudogap-enhanced paramagnetism is substantial but only for the d -wave case.

Fig.5(a) presents a plot of the orbital susceptibility for an s -wave gap and a tight-binding dispersion normalized by χ_{NS} , which is defined as in previous figures. The four curves correspond to the gap values $\Delta_{pg} = 0, 30, 60$, and 90 meV. The lattice dispersion Eq.20 is used with

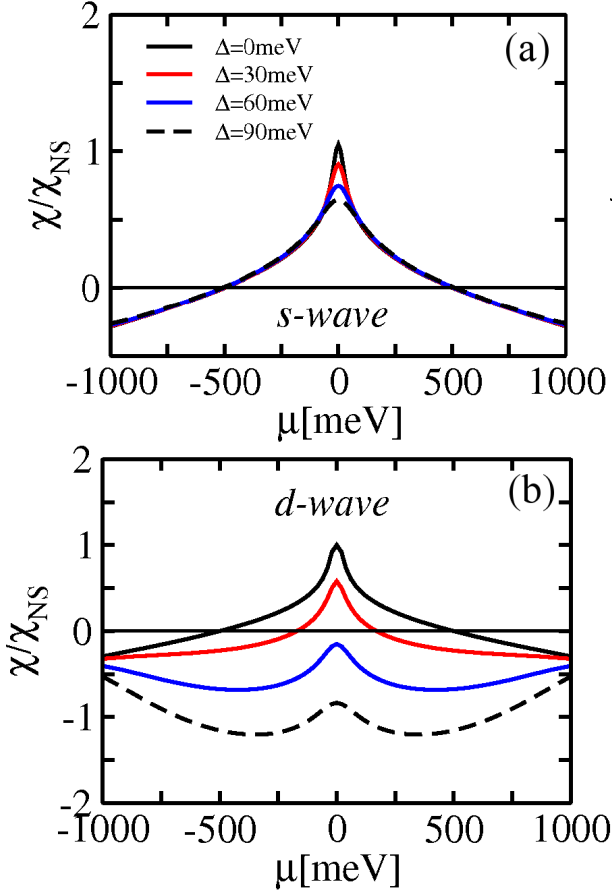


Figure 5: (left) The orbital susceptibility for a tight-binding dispersion with an *s*-wave order parameter. The normalization χ_{NS} is defined as the value of χ^{dia} in the normal state when $\mu = 0$. The curves correspond to gap sizes $\Delta_{pg} = 0, 30, 60, 90$ meV. There is very little change of χ^{dia} regardless of the gap size. (right) The orbital susceptibility for a tight-binding dispersion with a *d*-wave order parameter normalized by χ_{NS} . The *d*-wave form factor and the resulting enhancement in the size of the pairs leads to a significant enhancement of the diamagnetism for ranges of μ away from the Van-Hove point as the gap size increases.

$t = -300\text{meV}$ and $t' = 0$. The *s*-wave pairing gap has little effect on χ^{dia} , with all four curves tending to overlap except near the Van-Hove point at $\mu \approx 0$. The curves are entirely paramagnetic for a significant range of filling and the diamagnetic features at other filling are relatively small: an *s*-wave gap on a lattice is not enough to capture the observed experimental effects.

The corresponding figure for a *d*-wave gap is displayed in Fig.5(b). Gap and dispersion parameters that are identical to the *s*-wave parameters are used here. It is immediately seen that there is a significant enhancement of the diamagnetic susceptibility as the magnitude of the *d*-wave order parameter is increased. The Van-Hove point suppresses the extent of the diamagnetism

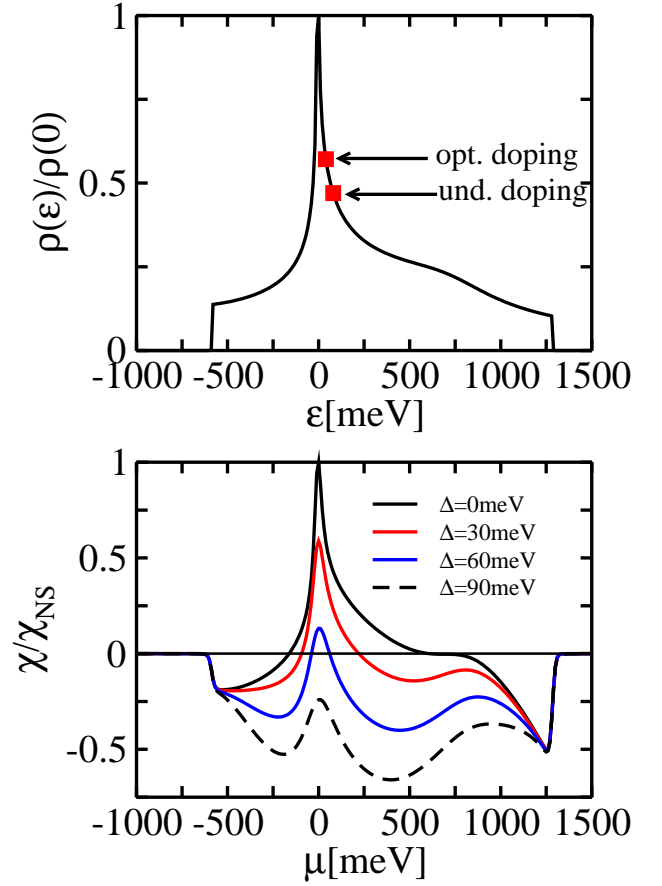


Figure 6: The behavior of the diamagnetism in a cuprate-like bandstructure. (upper panel) The model density of states showing that the Van-Hove point occurs at negative energies. Optimally doped samples have chemical potentials closer to the Van-Hove point than underdoped samples, as indicated by the arrows. (lower panel) The diamagnetic susceptibility as a function of μ for $\Delta_{pg} = 0, 30, 60$, and 90meV normalized by the value of the normal state χ^{dia} at $\mu = 0$.

and results in paramagnetism for small gap values and fillings near $\mu = 0$; nevertheless, the diamagnetism persists over a wide range of filling for each of the gap values considered here. For fillings that are near mid-band (i.e. $\mu \approx 500\text{meV}$), it is seen that there is a substantial increase in χ^{dia} as compared to the normal state once a finite Δ_{pg} is considered. The extent of this enhancement increases as one moves away from the Van-Hove point, mirroring the experimentally observed trend of the anomalous diamagnetism having the greatest impact in underdoped samples.

We turn now to more realistic parameters for the bandstructure of the cuprates in Fig.6. Here we use the ARPES-derived parameters [26] for Bi2212. With next nearest neighbor contributions one sees the broad trends are consistent with the earlier results. Note that the finite t' breaks particle hole symmetry and shifts the Van-Hove

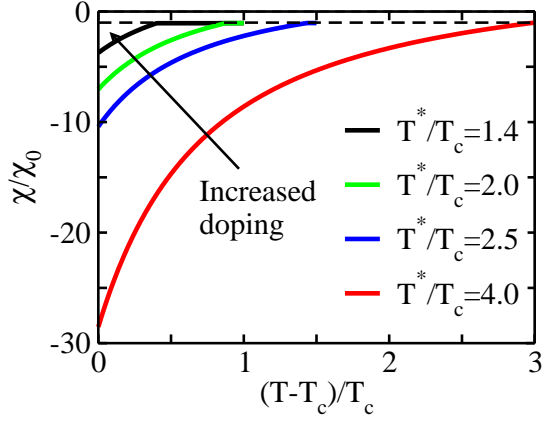


Figure 7: The diamagnetism as a function of temperature for different “hole concentrations” parameterized via T^*/T_c . The dashed line shows the normal state value of the susceptibility. This diamagnetism is to be associated with the large transport response from pairs or bosons near condensation. We contrast the present precursor superconductivity scenario with the more widely discussed phase fluctuation approach where the diamagnetism is associated with mesoscopic supercurrents.

point in the density of states.

Fig.6(a) indicates a typical density of states for a cuprate system, along with the estimated positions for the chemical potentials. Here the Van-Hove point is located at negative energies. The general trend is that optimally doped systems will be closer to the Van-Hove point than underdoped systems ([26]). Interestingly, this along with the stronger pseudogap in the underdoped case leads us to anticipate that underdoping enhances diamagnetism. The resulting orbital susceptibility is plotted in Fig.6(b) as a function of band filling for $\Delta = 0, 30, 60$, and 90meV . The curves are qualitatively similar to previous figures with the normal state χ^{dia} having both regions of paramagnetism and diamagnetism and becoming entirely diamagnetic for a sufficiently large value of Δ_{pg} .

Temperature Dependence of Diamagnetism

The above discussion has been quite general; we have essentially explored the consequences of Eq. (2) in all its generality. One can then inquire as to how this applies to the high temperature superconductors. This requires that we establish the parameters $\Delta_{pg}(T)$ and the fermionic chemical potential, $\mu(T)$. Here, for definiteness we use our preformed pair scenario [27] which is based on stronger than BCS attractive interactions (consistent with small pair size and anomalously high pairing onset temperature T^*). Once the pseudogap and chemical potential parameters are self consistently obtained [27], one accommodates a variety of dopings, by effectively fitting [27] the attractive interaction to match T^* and

T_c . For definiteness, we presume the band dispersion is associated with $t = 300\text{meV}$ and $\mu = -1.75t$, chosen somewhat away from the Van Hove point.

We present temperature dependent plots of the diamagnetic response χ^{dia} , in Figure 7 for four different dopings. Each curve is normalized by its normal state value, which is separately plotted as a dashed line. Independently of the particular parameters that are used, it is seen that the magnitude of χ^{dia} is enhanced even at temperatures well above T_c . Importantly, this diamagnetism is not restricted to two dimensional models, as in fluctuation theories. Experiments as well re-enforce three dimensional critical behavior [28–30].

In this way the present physical picture contrasts with the traditional fluctuation approach, in which one might expect large diamagnetism but only in the narrow critical regime. Here, it is the stronger than BCS attraction which stabilizes these pair degrees of freedom (up to high temperatures $T \approx T^*$) rather than the low dimensionality [12]. Importantly, in the present theory we compute the total conductivity based on the pseudogap self energy, not the fluctuation corrections and in this way are analytically able to establish compatibility with the conductivity sum rules.

COMPARISON BETWEEN DIAMAGNETISM AND CONDUCTIVITY

The orbital susceptibility is not the only transport property which can be associated with the pseudogap self energy of Eq. (1). We have previously discussed the optical and THz conductivity [22, 23]. Here we concentrate on the challenges raised by recent experimental papers [31, 32] which have pointed out the seemingly contradictory behavior implicit in the dissipative conductivity and the orbital susceptibility. The authors of Ref. 31 deduce “However, if the diamagnetism signal above T_c is solely due to superconducting correlations then it is a well posed challenge to explain the lack of straightforward correspondence to conductivity.” In this section, we address this challenge by looking simultaneously at the linear diamagnetic response and the dissipative conductivity.

In this regard, it is important here to incorporate the ordered phase. We can anticipate that we now have two distinct contributions to the fermionic self energy $\Sigma(\mathbf{k}, \omega)$

$$\begin{aligned} \Sigma(\mathbf{k}, \omega) &= \Sigma_{pg, \mathbf{k}} + \Sigma_{sc, \mathbf{k}} \\ &= -i\gamma + \frac{\Delta_{pg, \mathbf{k}}^2}{\omega + \xi_{\mathbf{k}} + i\gamma} + \frac{\Delta_{sc, \mathbf{k}}^2}{\omega + \xi_{\mathbf{k}}} . \end{aligned} \quad (21)$$

The first of these is associated with the normal state and the second with the condensate.

Following the analysis of this paper (above T_c) we may similarly arrive at the below T_c counterpart directly from

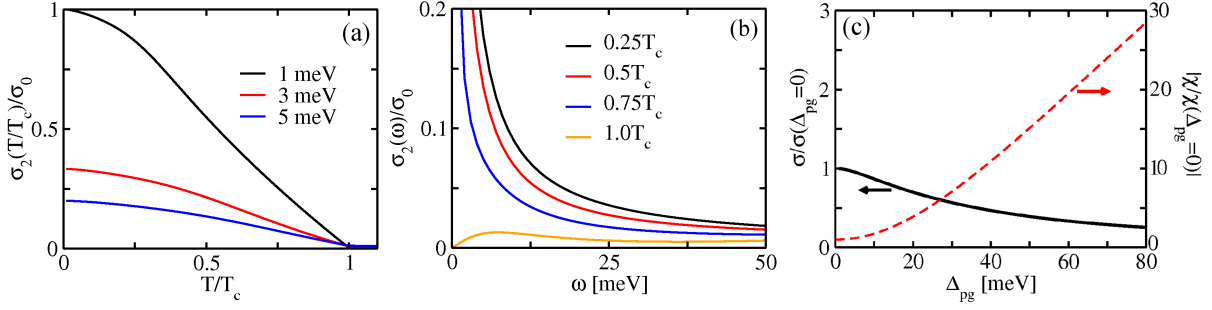


Figure 8: Numerically generated plots of (a) the imaginary conductivity σ_2 as a function of temperature at constant energy ω . The curves are normalized by σ_0 , the value of σ_2 at zero temperature with $\omega = 1\text{meV}$. (b) The imaginary conductivity σ_2 as a function of frequency for constant temperature T . The curves are again normalized by σ_0 . (c) The conductivity and diamagnetic susceptibility as functions of Δ_{pg} at $k_B T = 15\text{meV}$.

this self energy. Here for simplicity we rewrite $\vec{P}(Q)$ in the regime of very weak dissipation ($\gamma \approx 0$) and s -wave pairing where the behavior is more physically transparent.

$$\begin{aligned} \vec{P}(\omega, \mathbf{q}) = & \sum_{\mathbf{k}} \frac{\mathbf{k}\mathbf{k}}{m^2} \left[\frac{E_+ + E_-}{E_+ E_-} (1 - f_+ - f_-) \right. \\ & \times \frac{E_+ E_- - \xi_+ \xi_- - \delta \Delta^2}{\omega^2 - (E_+ + E_-)^2} - \frac{E_+ - E_-}{E_+ E_-} \\ & \left. \times \frac{E_+ E_- + \xi_+ \xi_- + \delta \Delta^2}{\omega^2 - (E_+ - E_-)^2} (f_+ - f_-) \right], \end{aligned} \quad (22)$$

where $f_{\pm} = f(E_{\pm})$ and $\delta \Delta^2 = \Delta_{sc}^2 - \Delta_{pg}^2$, $\xi_{\pm} = \xi_{\mathbf{k} \pm \mathbf{q}/2}$, and $E_{\pm} = E_{\mathbf{k} \pm \mathbf{q}/2}$. The transverse sum rule can be shown to be precisely satisfied, below as well as above T_c . The longitudinal sum rule cannot be easily proved below T_c , (due to collective mode effects) although it is analytically satisfied in the normal state as shown earlier in this paper.

Our interest here is on contrasting the diamagnetism with the dissipative conductivity

$$\sigma_2(\omega) = \lim_{\mathbf{q} \rightarrow 0} \text{Re} \left[\frac{P_{xx}(\mathbf{q}, \omega) + (n/m)_{xx}}{i\omega} \right] \quad (23)$$

where the imaginary counterpart corresponds to the real part of the frequency dependent conductivity σ_1 . Note that Eqs. (2) and (23) are superficially rather similar, but importantly very different. This difference derives from the different denominators and in a related fashion, the order of $\mathbf{q}, \omega \rightarrow 0$ limits.

We stress that our below T_c extension can be derived microscopically [27, 33, 34]. However, the present more general approach based on the self energy indicates that the results should be rather generic. In support of this below- T_c generalization of the self energy, it is straightforward to see from Eq. (21) how the Fermi arcs will collapse to point nodes as soon as the system passes below T_c [10] and that the general 2-gap phenomena, in which the nodal region is sensitive to Δ_{sc} while the antinode region exhibits little temperature dependence [11] are all

direct consequences. In the same way one can explore the optical conductivity [22] and THz conductivity [23], all of which are highly constrained by the simple self energy expression in Eq. (1) and its extension below T_c in Eq. (21). In addition, these expressions for the self energy lead to results for the specific heat [35] and serve to constrain the tunneling characteristics, including quasi-particle interference [36]. Because the measured diamagnetism seems to be well correlated with the Nernst effect, it is important to note that a large Nernst response was addressed earlier and argued [37] to be associated with pre-formed pairs, as distinguished from normal state vortices.

It is of interest then to compare the behavior of the conductivity and the diamagnetic response. Fig.8 displays our results for the cuprate models, based on Eqs. (2) and (23). Fig.8(a) shows how the normal state $\sigma_2(\omega)$ behaves as a function of temperature for three different low frequencies and Fig.8(b) plots the imaginary conductivity σ_2 as a function of frequency for a range of different temperatures. At roughly T_c , we find that σ_2 shows a sharp upturn at low ω . Below T_c we find the expected superfluid frequency dependence $\sigma_2 \propto n_s/\omega$.

We find that $\sigma_2(\omega)$ is modestly increasing with increasing ω above T_c as seen in experiment, albeit slightly away from the transition. Experimental studies do reveal a small 10-15K range where a fluctuation contribution is visible. But except in this narrow temperature region, the observed behavior is not compatible with that expected of a phase fluctuation contribution, where a ω^{-1} dependence would occur [38], presumably over the same range of temperatures as the enhanced diamagnetic response. Both derive from the same mesoscopic supercurrents. The absence of significant σ_2 contributions above T_c in the present theory is related to the fact that the pseudogap does not contribute to the superfluid density. Our derivation of the current-current correlation function centered on this important constraint. Thus, it should not be surprising that we find little signature of the superfluid density in σ_2 of the normal phase. Here, more-

over, fluctuation effects are not present since ours is basically a mean field approach. As speculated in Ref. 31, one should distinguish these near T_c critical fluctuations from preformed pairs that persist to much higher temperatures closer to T^* .

It is notable that even σ_1 is suppressed in the low frequency regime, when a pseudogap is present. This is because there are fewer fermions available to contribute to transport; their number is reduced since they are tied up into pairs. However, once the frequency is sufficiently high to break the pairs into individual fermions, the conductivity rises, leading [22] to a second peak at higher $\omega \approx 2\Delta$ in $\sigma_1(\omega)$. One can think of this two component behavior (which is observed experimentally [39]) as reflecting a transfer of spectral weight as implied by the conductivity f-sum rule. The behavior of $\sigma_2(\omega)$, shown in Fig. 8(b) is rather similarly constrained by these same effects. On general principles, σ_2 must vanish at strictly zero frequency as long as the system is normal. Here, too, the low frequency behavior is suppressed by the presence of a pseudogap as a result of the gap-induced decrease in the number of carriers. The second peak in σ_1 which reflects the breaking of pairs, leads, via a Kramers Kronig transform to a slight depression in $\sigma_2(\omega)$ in this frequency regime. Thus, $\sigma_2(\omega)$ is significantly reduced relative to a traditional Fermi liquid.

Fig.8(c) compares the effects of a d -wave pseudogap on the diamagnetism and dc conductivity. Here we presume that the chemical potential of the underdoped cuprates is somewhat away from the Van Hove points, to avoid the large normal state *paramagnetism* [40]. The left and right hand axes plot the zero frequency conductivity as a function of varying pseudogap energy scale Δ_{pg} and the orbital susceptibility with varying Δ_{pg} respectively. Once pre-formed pairs are present, the diamagnetic contribution is significantly enhanced, relative to the very weak band diamagnetism found at $\Delta_{pg} = 0$.

These observations suggest an important anti-correlation between the dc conductivity and the orbital susceptibility in the pseudogap phase, which is shown in Fig.8(c). The dc conductivity is reduced with increasing Δ_{pg} due to the opening of a gap in the fermionic spectrum. By contrast the existence of bosonic degrees of freedom (in the vicinity of condensation) and d -wave pairing allows for an enhanced diamagnetic response.

CONCLUSION

Because of the rather widespread adoption [3–6] of a broadened BCS form for the pseudogap self energy (as given in Eq. (1)), it seems appropriate to explore the consequences for transport, and in particular diamagnetism. We have done so here in a fashion which is rather independent of the microscopic details. The logic we followed is straightforward. We used the absence of a normal state

Meissner effect to constrain the $q = 0, \omega = 0$ component of the current-current correlation function $\overleftrightarrow{P}(0,0)$. We extended this correlation function to finite 4-vector arguments $\overleftrightarrow{P}(Q)$ in a fashion which analytically satisfies the f-sum rules, and yields known results for limiting cases. This correlation function expanded for small wavevector, then, directly yields the orbital susceptibility, associated with the pseudogap self energy.

In this way, our numerical studies are expected to yield rather generic results, a main summary of which is presented in Figure 1. The orbital susceptibility associated with a tightbinding bandstructure is very different from more familiar Landau diamagnetism [20] and, importantly, near Van Hove singularities this susceptibility is paramagnetic. However, the effect of a pseudogap can lead to large negative corrections to the bandstructure predictions, for the d wave case. That such diamagnetism is present only for d -wave symmetry is due in part to the presence of nodal fermions and to the extended size of the d -wave pairs.

It is of interest to contrast our approach with other theories in the literature. Podolsky et al. [41] and Eckl and Hanke [38] have respectively applied phase fluctuation approaches to address diamagnetism and conductivity experiments leading to several predictions: (i) that [38] the closely related $\sigma_2(\omega) \propto \omega^{-1}$, at sufficiently high ω . (ii) that [41], the underdoped cuprates behave as a dilute vortex liquid over a wide range of temperatures above T_c . More recently, however, there has been some concern raised [32] about this vortex plasma model for the cuprates. A comparison of the conductance and orbital susceptibility suggests that these vortices must exhibit an anomalously large vortex diffusion constant. We note that these concerns do not apply to the present approach to transport. Also notable is a large body of work on related vortex scenarios[42, 43], as well as theoretical studies [44] which address the superconducting fluctuation contribution to conductivity and diamagnetism in the presence of current-current interactions in the t-J model.

The calculations we present here are different primarily because we consider non-Fermi liquid aspects to be dominant. We have shown how a large diamagnetic (linear) response derives in part from the well known enhanced transport contribution associated with bosons near condensation. At the same time, in the present theory, these bosons are meta-stable at temperatures much higher than in the critical regime, away from where standard fluctuation theories apply. This high temperature stability is due to stronger-than-BCS attractive interactions. We caution that this lattice diamagnetism is associated with two constraints: that the pairing be d -wave and that the (near mid-band) chemical potential μ lie away from the Van Hove singularities. When μ is at the Van Hove point, the strong paramagnetism of the normal state [40] in-

hibits a diamagnetic response, as does s -wave pairing in a tight binding band.

In summary, this preformed pair pseudogap scenario leads to very different behavior for the conductivity and the diamagnetism and this appears to bear on recent, otherwise challenging experiments [31, 32]. In the former case because there are fewer fermions around to contribute to the $\omega = 0$ conductivity (they are tied up into “bosons”) this leads to a reduction in the dissipative contribution to the conductivity. Because we are working at effectively zero magnetic field, we have not addressed diamagnetism associated with a non-linear response, although this appears to be very anomalous experimentally [45]. We end by reiterating that our starting point, Eq. (1), for deriving $\sigma(\omega)$ and χ^{dia} is frequently adopted

in the literature so our results should have a wider applicability and generality.

This work is supported by NSF-MRSEC Grant 0820054. We thank Hao Guo and Chih-Chun Chien for valuable insights, and Dr. Guo for the analytic proof of the longitudinal f-sum rule.

Appendix A: Effects of finite γ

The current-current correlation function will be discussed below in the normal state in the presence of lifetime γ^{-1} , which is kept arbitrary in the analysis.

The starting point in the derivation of the current-current correlation function $\overleftrightarrow{P}(\mathbf{q}, i\Omega_m)$ is the phenomenological cuprate self-energy $\Sigma_{pg,K}$ as determined by ARPES experiments. It takes the form

$$\Sigma_{pg,K} = -i\gamma \text{sgn}\omega_n + \frac{\Delta_{pg,\mathbf{k}}^2}{i\omega_n + \xi_{\mathbf{k}} + i\gamma \text{sgn}\omega_n} \quad (24)$$

where $K = (\mathbf{k}, i\omega_n)$ is a 4-vector, $i\omega_n$ is a fermionic Matsubara frequency, $\xi_{\mathbf{k}}$ is the normal state fermion dispersion, γ^{-1} is the pseudogap pair lifetime, $\text{sgn}(\dots)$ denotes the sign function, and $\Delta_{pg,\mathbf{k}} \equiv \Delta_{pg}\varphi_{\mathbf{k}}$ where Δ_{pg} is the magnitude of the pseudogap and $\varphi_{\mathbf{k}}$ is the gap form factor. Eq.24 is the generalization of the phenomenological $\Sigma_{pg,K}$ to finite temperature, rather than the $i\omega_n \rightarrow \omega + i0^+$ limit that it is normally displayed in. The other physical constraint that will be used is the absence of the Meissner effect above T_c . This condition is expressed

$$\overleftrightarrow{P}(0,0) + \frac{\overleftrightarrow{n}}{m} = 0 \quad (25)$$

and relates the zero momentum and frequency current-current correlation function to \overleftrightarrow{n}/m . Eq.25 allows one to avoid issues of Ward identities and renormalization of the bare electromagnetic vertex when deriving $\overleftrightarrow{P}(0,0)$ because the tensor \overleftrightarrow{n}/m is defined solely in terms of the normal state dispersion $\xi_{\mathbf{k}}$ and the Green's function G_K . By incorporating Eq.24, Eq.25 can be used to calculate the electromagnetic vertex renormalization by first rewriting \overleftrightarrow{n}/m

$$\frac{\overleftrightarrow{n}}{m} = 2 \sum_K \frac{\partial^2 \xi_{\mathbf{k}}}{\partial \mathbf{k} \partial \mathbf{k}} G_K = -2 \sum_K \frac{\partial \xi_{\mathbf{k}}}{\partial \mathbf{k}} \frac{\partial G_K}{\partial \mathbf{k}} \quad (26)$$

where the second equality follows from an integration by parts. The derivative of the Green's function can be written in terms of a bare Green's function and Eq.24

$$\frac{\partial G_K}{\partial \mathbf{k}} = -G_K^2 \frac{\partial G_K^{-1}}{\partial \mathbf{k}} = G_K^2 \left(\frac{\partial \xi_{\mathbf{k}}}{\partial \mathbf{k}} + \frac{\partial \Sigma_{pg,K}}{\partial \mathbf{k}} \right) \quad (27)$$

Inserting Eq.27 into Eq.26 yields

$$\frac{\overleftrightarrow{n}}{m} = -2 \sum_K G_K^2 \frac{\partial \xi_{\mathbf{k}}}{\partial \mathbf{k}} \frac{\partial \xi_{\mathbf{k}}}{\partial \mathbf{k}} \left(1 - \Delta_{pg,\mathbf{k}}^2 G_{0,-K}^\gamma \right) \quad (28)$$

where $G_{0,K}^\gamma$ is defined

$$G_{0,K}^\gamma \equiv \frac{1}{i\omega_n - \xi_{\mathbf{k}} + i\gamma \text{sgn}\omega_n} \quad (29)$$

and takes the appearance of a normal state Green's function with a self-energy contribution due to a scattering process resulting in the $i\gamma$ factor. Eq.28 implies that the zero momentum and zero frequency current-current correlation function is

$$\overleftrightarrow{P}(0,0) = 2 \sum_K G_K^2 \frac{\partial \xi_{\mathbf{k}}}{\partial \mathbf{k}} \frac{\partial \xi_{\mathbf{k}}}{\partial \mathbf{k}} \left(1 - \Delta_{pg,\mathbf{k}}^2 G_{0,-K}^\gamma \right)^2 \quad (30)$$

The key observation to make of Eq.30 is that (i) the phenomenological self-energy and (ii) ensuring the absence of a Meissner effect above T_c were sufficient assumptions to calculate the renormalization of the bare electromagnetic vertex $\lambda_{\mathbf{k}}$ in the $\mathbf{q}, i\Omega_m = 0$ limit, namely that the dressed electromagnetic vertex $\Lambda_{\mathbf{k}}$ is

$$\lambda_{\mathbf{k}} = \frac{\partial \xi_{\mathbf{k}}}{\partial \mathbf{k}} \rightarrow \Lambda_{\mathbf{k}} = \frac{\partial \xi_{\mathbf{k}}}{\partial \mathbf{k}} \left(1 - \Delta_{pg,\mathbf{k}}^2 G_{0,-K}^\gamma \right) \quad (31)$$

The transport properties derived from Eq.31 and its extension to finite momentum \mathbf{q} are of very general character in describing the pseudogap state. The remaining step is the extension of Eq.30 to finite \mathbf{q} and $i\Omega_m$ which will be accomplished at this stage by analogy to the BCS current-current correlation function but will be supplemented by an analytic proof of the transverse f-sum rule that depends on the $i\Omega_m$ dependence of $\overleftrightarrow{P}(\mathbf{q}, i\Omega_m)$. One can utilize the \mathbf{q} and $i\Omega_m$ dependences in BCS theory to build further confidence by noting that the correction to the bare electromagnetic vertex is of the BCS-form but with opposite sign. Mirroring the \mathbf{q} and $i\Omega_m$ dependence of $\lambda_{\mathbf{k}}$, the Green's function, and the correction to $\lambda_{\mathbf{k}}$, the extension of Eq.30 is

$$\overleftrightarrow{P}(\mathbf{q}, i\Omega_m) = 2 \sum_K G_K G_{K+Q} \frac{\partial \xi_{\mathbf{k}-\mathbf{q}/2}}{\partial \mathbf{k}} \frac{\partial \xi_{\mathbf{k}-\mathbf{q}/2}}{\partial \mathbf{k}} \left(1 - \Delta_{pg,\mathbf{k}} \Delta_{pg,\mathbf{k}+\mathbf{q}} G_{0,-K}^\gamma G_{0,-K-Q}^\gamma \right) \quad (32)$$

The analogy between Eq.32 and its BCS counterpart can be further exploited by introducing the function $F_{pg,K}$, defined as

$$F_{pg,K} \equiv \Delta_{pg,\mathbf{k}} G_{0,-K}^\gamma G_K \quad (33)$$

While this is of similar form to the anomalous propagator $F_{sc,K}$, $F_{pg,K}$ *does not* reflect phase coherent pairs. Inserting Eq.33 into Eq.32 leads to a compact form

$$\overleftrightarrow{P}(\mathbf{q}, i\Omega_m) = 2 \sum_K \frac{\partial \xi_{\mathbf{k}-\mathbf{q}/2}}{\partial \mathbf{k}} \frac{\partial \xi_{\mathbf{k}-\mathbf{q}/2}}{\partial \mathbf{k}} \left(G_K G_{K+Q} - F_{pg,K} F_{pg,K+Q} \right) \quad (34)$$

The proof of the transverse sum rule will be facilitated by working with the spectral representations of G_K and $F_{pg,K}$, which are implicitly defined through the relations

$$G_K = \int \frac{d\omega}{2\pi} \frac{A_G(\mathbf{k}, \omega)}{i\omega_n - \omega} \quad (35)$$

$$F_{pg,K} = \int \frac{d\omega}{2\pi} \frac{A_{F_{pg}}(\mathbf{k}, \omega)}{i\omega_n - \omega} \quad (36)$$

Inserting Eq.35 into Eq.32 leads to the result

$$\begin{aligned} \overleftrightarrow{P}(\mathbf{q}, i\Omega_m) = & 2 \sum_{\mathbf{k}} \frac{\partial \xi_{\mathbf{k}-\mathbf{q}/2}}{\partial \mathbf{k}} \frac{\partial \xi_{\mathbf{k}-\mathbf{q}/2}}{\partial \mathbf{k}} \int \frac{d\omega d\omega'}{(2\pi)^2} \left(\frac{f(\omega) - f(\omega')}{\omega - \omega' + i\Omega_m} \right) \\ & \times \left(A_G(\mathbf{k}, \omega) A_G(\mathbf{k} + \mathbf{q}, \omega') - A_{F_{pg}}(\mathbf{k}, \omega) A_{F_{pg}}(\mathbf{k} + \mathbf{q}, \omega') \right) \end{aligned} \quad (37)$$

The current-current correlation function can be further simplified by replacing one of the spectral functions in each

term with the full G or F_{pg} function, resulting in the final expression

$$\begin{aligned} \overleftrightarrow{P}(\mathbf{q}, i\Omega_m) = & 2 \sum_{\mathbf{k}} \frac{\partial \xi_{\mathbf{k}-\mathbf{q}/2}}{\partial \mathbf{k}} \frac{\partial \xi_{\mathbf{k}-\mathbf{q}/2}}{\partial \mathbf{k}} \int \frac{d\omega}{2\pi} f(\omega) \\ & \times \left(A_G(\mathbf{k}) G(\mathbf{k} + \mathbf{q}, \omega + i\Omega_m) + A_G(\mathbf{k} + \mathbf{q}, \omega) G(\mathbf{k}, \omega - i\Omega_m) \right. \\ & \left. - A_{F_{pg}}(\mathbf{k}) F_{pg}(\mathbf{k} + \mathbf{q}, \omega + i\Omega_m) - A_{F_{pg}}(\mathbf{k} + \mathbf{q}, \omega) F_{pg}(\mathbf{k}, \omega - i\Omega_m) \right) \end{aligned} \quad (38)$$

Next we prove the transverse f-sum rule in the pseudogap state for this more general case of arbitrary dissipation. Recall that the f-sum rule is expressed

$$\lim_{\mathbf{q} \rightarrow 0} \int \frac{d\Omega}{\pi} \left(-\frac{1}{\Omega} \text{Im} \overleftrightarrow{P}(\mathbf{q}, \Omega^+) \right) = \frac{\overleftrightarrow{n}}{m} \quad (39)$$

where $\Omega^+ = \Omega + i0^+$.

From Eq. (28) we have

$$\begin{aligned} \frac{\overleftrightarrow{n}}{m} = & -2 \sum_K \frac{\partial \xi_{\mathbf{k}}}{\partial \mathbf{k}} \frac{\partial \xi_{\mathbf{k}}}{\partial \mathbf{k}} \left(G_K^2 - F_{pg,K}^2 \right) \\ = & -2 \sum_{\mathbf{k}} \frac{\partial \xi_{\mathbf{k}}}{\partial \mathbf{k}} \frac{\partial \xi_{\mathbf{k}}}{\partial \mathbf{k}} \int \frac{d\omega d\omega'}{(2\pi)^2} \left(f(\omega) - f(\omega') \right) \\ & \times \frac{A_G(\mathbf{k}, \omega) A_G(\mathbf{k}, \omega') - A_{F_{pg}}(\mathbf{k}, \omega) A_{F_{pg}}(\mathbf{k}, \omega')}{\omega - \omega'} \end{aligned} \quad (40)$$

From Eq. (34) we have

$$\begin{aligned} \frac{1}{\pi\Omega} \text{Im} \overleftrightarrow{P}(0, \Omega^+) = & -2 \sum_{\mathbf{k}} \frac{\partial \xi_{\mathbf{k}}}{\partial \mathbf{k}} \frac{\partial \xi_{\mathbf{k}}}{\partial \mathbf{k}} \int \frac{d\omega}{2\pi} \frac{f(\omega)}{\Omega} \\ & \times \left(A_G(\mathbf{k}, \omega) A_G(\mathbf{k}, \omega + \Omega) - A_{F_{pg}}(\mathbf{k}, \omega) A_{F_{pg}}(\mathbf{k}, \omega + \Omega) \right) \end{aligned} \quad (41)$$

Thus

$$\begin{aligned} \int \frac{d\Omega}{\pi} \left(-\frac{1}{\Omega} \text{Im} \overleftrightarrow{P}(\mathbf{q}, \Omega) \right) = & 2 \sum_{\mathbf{k}} \frac{\partial \xi_{\mathbf{k}}}{\partial \mathbf{k}} \frac{\partial \xi_{\mathbf{k}}}{\partial \mathbf{k}} \int \frac{d\omega}{2\pi} \frac{d\omega'}{\pi} \frac{f(\omega)}{\omega' - \omega} \\ & \times \left(A_G(\mathbf{k}, \omega) A_G(\mathbf{k}, \omega') - A_{F_{pg}}(\mathbf{k}, \omega) A_{F_{pg}}(\mathbf{k}, \omega') \right) \\ = & -\frac{\overleftrightarrow{n}}{m} \end{aligned} \quad (42)$$

which leads to the desired result.

[1] R. Daou, J. Chang, D. LeBoeuf, O. Cyr-Choiniere, F. Laliberte, N. Doiron-Leyraud, B. J. Ramshaw, R. Liang, D. A. Bonn, W. Hardy, et al., *Nature* **463**, 519 (2010).

[2] V. Hinkov, P. Bourges, S. Pailhes, Y. Sidis, A. Ivanov, C. D. Frost, T. G. Perring, C. T. Lin, D. P. Chen, and B. Keimer, *Nature Physics* **3**, 780 (2007).
 [3] B. Jankó, J. Maly, and K. Levin, *Phys. Rev. B* **56**, R11407, (1997); J. Maly, B. Jankó, and K. Levin, *Physica C* **321**, 113 (1999) and cond-mat/9710187.
 [4] M. R. Norman, M. Randeria, H. Ding, and J. C. Campuzano, *Phys. Rev. B* **57**, 11093(R) (1998).
 [5] T. Senthil and P. A. Lee, *Phys. Rev. B* **79**, 245116 (2009).

- [6] A. V. Chubukov, M. R. Norman, A. J. Millis, and E. Abrahams, Phys. Rev. B **76**, 180501(R) (2007).
- [7] L. Li, Y. Wang, S. Komiya, S. Ono, Y. Ando, G. D. Gu, and N. P. Ong, Phys. Rev. B **81**, 054510 (2010).
- [8] L. Li, Y. Wang, M. J. Naughton, S. Ono, Y. Ando, and N. P. Ong, Europhys. Lett. **72**, 451 (2005).
- [9] Y. Wang, Z. A. Xu, T. Kakeshita, S. Uchida, S. Ono, Y. Ando, and O. N. P, Phys. Rev. B **64**, 224519 (2001).
- [10] Q. Chen and K. Levin, Phys. Rev. B. **78**, 0200513(R) (2008).
- [11] C.-C. Chien, Y. He, and K. Levin, Phys. Rev. B **79**, 214527 (2009).
- [12] A. I. Larkin and A. A. Varlamov, *Theory of Fluctuations in Superconductors* (Oxford University Press, New York, 2005).
- [13] V. Oganesyan, D. A. Huse, and S. L. Sondhi, Phys. Rev. B **73**, 094503 (2006).
- [14] I. Ussishkin, S. Sondhi, and D. A. Huse, Phys. Rev. Lett. **89**, 287001 (2002).
- [15] A. S. Alexandrov, J. Phys.: Condens. Matter **22**, 426003 (2010).
- [16] P. W. Anderson, Nature Phys. **3**, 160 (2007).
- [17] J. D. Sau and S. Tewari, Phys. Rev. Lett. **107**, 177006 (2011).
- [18] N. W. Ashcroft and N. D. Mermin, *Solid State Physics* (Thomson Learning, USA, 1976).
- [19] A. Schmid, Phys. Rev. **180**, 527 (1969).
- [20] P. Skudlarski and G. Vignale, Phys. Rev. B **43**, 5764 (1991).
- [21] A. L. Fetter and J. D. Walecka, *Quantum Theory of Many-Particle Systems* (McGraw-Hill, San Francisco, 1971).
- [22] D. Wulin, H. Guo, C.-C. Chien, and K. Levin, eprint, arXiv:1108.4375.
- [23] D. Wulin, V. Mishra, and K. Levin, eprint, arXiv:1112.5098.
- [24] L. Benfatto, A. Toschi, S. Caprara, and C. Castellani, Phys. Rev. B **66**, 054515 (2002).
- [25] Q. J. Chen, Ph.D. thesis, University of Chicago (2000), (unpublished).
- [26] A. Piriou, N. Jenkins, C. Berthod, I. Maggio-Aprile, and F. O, Nature Comm. **2:221**, 1 (2011).
- [27] Q. J. Chen, J. Stajic, S. N. Tan, and K. Levin, Phys. Rep. **412**, 1 (2005).
- [28] S. Kamal, D. A. Bonn, N. Goldenfeld, P. J. Hirschfeld, R. Liang, and W. N. Hardy, Phys. Rev. Lett. **73**, 1845 (1994).
- [29] N. Overend, M. Howson, and I. Lawrie, Phys. Rev. Lett. **72**, 3238 (1994).
- [30] P. Pureur, R. Menegotto Costa, P. Rodrigues, J. Schaf, and J. V. Kunzler, Phys. Rev. B **47**, 11420 (1993).
- [31] L. S. Bilbro, R. V. Guilar, B. Logvenov, O. Pelleg, I. Bozovic, and N. P. Armitage, Nature Physics **7**, 2980302 (2011).
- [32] L. S. Bilbro, R. V. Guilar, B. Logvenov, I. Bozovic, and N. P. Armitage, Phys. Rev. B **84**, 100511(R) (2011).
- [33] Q. J. Chen, I. Kosztin, B. Jankó, and K. Levin, Phys. Rev. Lett. **81**, 4708 (1998).
- [34] I. Kosztin, Q. J. Chen, Y.-J. Kao, and K. Levin, Phys. Rev. B **61**, 11662 (2000).
- [35] Q. J. Chen, K. Levin, and I. Kosztin, Phys. Rev. B **63**, 184519 (2001).
- [36] D. Wulin, Y. He, C.-C. Chien, D. K. Morr, and K. Levin, Phys. Rev. B **80**, 134504 (2009).
- [37] S. Tan and K. Levin, Phys. Rev. B **69**, 064510 (2004).
- [38] T. Eckl and W. Hanke, Phys. Rev. B **74**, 134510 (2006).
- [39] Y. S. Lee, K. Segawa, Z. Q. Li, W. J. Padilla, M. Dumm, S. V. Dordevic, C. C. Homes, Y. Anod, and D. N. Basov, Phys. Rev. B **72**, 054529 (2005).
- [40] P. Skudlarski and G. Vignale, Phys. Rev. B **43**, 5764 (1991).
- [41] D. Podolsky, S. Raghu, and A. Vishwanath, Phys. Rev. Lett. **99**, 117004 (2007).
- [42] P. A. Lee, Physica C **388-389**, 7 (2003).
- [43] P. A. Lee, Phys. Rev. B **66**, 094513 (2002).
- [44] L. Benfatto, S. Caprara, and C. Di Castro, Eur. Phys. J. B **17**, 95 (2000).
- [45] L. Li, Y. Wang, S. Komiya, S. Ono, Y. Ando, G. G. Gu, and N. P. Ong, Phys. Rev. B **81**, 054510 (2010).